SRI International

Final Report • January 2000

CASE STUDY ANALYSES OF THE SUCCESS DC-8 SCANNING LIDAR DATABASE

Prepared by:

Edward E. Uthe, Principal Scientist
Optical Sensing Program
Applied Physical Sciences Laboratory

Prepared for:

National Aeronautics and Space Administration
Ames Research Center
Atmospheric Chemistry and Dynamics Br., 245-5
Moffett Field, California 94035-1000

Attn: Mr. Stephen Hipskind

SRI Project ESU-3268
Cooperative Agreement No. NAG2-1235

Approved by:

Eric M. Pearson, Director
Applied Physical Sciences Laboratory

CONTENTS

LIST OF FIGURES AND TABLES ii
LIST OF ABBREVIATIONS iii
SUMMARY iv
1 INTRODUCTION AND OBJECTIVE 1
2 DC-8 SCANNING LIDAR DATABASE 3
3 DATA PROCESSING METHODS 16
4 CASE STUDY ANALYSES 17
5 CONCLUSIONS AND RECOMMENDATIONS 23
6 PUBLICATIONS AND PRESENTATIONS 25
6.1 Journal Publications 25
6.2 Conference Presentations 25
APPENDIX A

FIGURE

1 DC-8 scanning lidar operation 2

TABLES

1 DC-8 scanning lidar SUCCESS operations log 5
2 DC-8 scanning lidar SUCCESS configuration and data inventory summary 10
3 DC-8 scanning lidar data digitization summary 11
4 DC-8 scanning lidar compact disk database 13
5 Angular scanning DC-8 lidar case studies 17

ABBREVIATIONS

AEAP	Atmospheric Effects of Aviation Program
SRI	SRI International
SUCCESS	subsonic aircraft contrail and cloud effects special study
ARM	Atmospheric Radiation Measurements
CART	Clouds and Radiation Testbed
CDs	compact disks
DADS	DC-8 data network

SUMMARY

Under project SUCCESS (Subsonic Aircraft Contrail and Cloud Effects Special Study) funded by the Atmospheric Effects of Aviation Program, SRI International (SRI) developed an angular scanning backscatter lidar for operation on the NASA DC-8 research aircraft and deployed the scanning lidar during the SUCCESS field campaign. The primary purpose of the lidar was to generate real-time video displays of clouds and contrails above, ahead of, and below the DC-8 as a means to help position the aircraft for optimum cloud and contrail sampling by onboard in situ sensors, and to help extend the geometrical domain of the in situ sampling records. A large, relatively complex lidar database was collected and several data examples were processed to illustrate the value of the lidar data for interpreting the other data records collected during SUCCESS. These data examples were used to develop a journal publication for the special SUCCESS *Geophysical Research Letters* issue (reprint presented as Appendix A). The data examples justified data analyses of a larger part of the DC-8 lidar database and is the objective of the current study.

Efficient processing of the SUCCESS DC-8 scanning lidar database required substantial effort to enhance hardware and software components of the data system that was used for the initial analyses. MATLAB instructions are used to generate altitude and distance color-coded lidar displays corrected for effects introduced by aircraft pitch and forward movement during an angular scan time interval. Onboard in situ sensor atmospheric measurements are propagated to distances ahead of the DC-8 using recorded aircraft velocity so that they can be plotted on the lidar displays for comparison with lidar remotely observed aerosol distributions. Resulting lidar and in situ sensor polar scan displays over extended sampling intervals are integrated into a time series movie format for 36 case studies and are playable at the web site www.rsed.sri.com/lidar.

Contrails and clouds were detected to ranges of 15 km by the forward-viewing angular scanning lidar and were progressively mapped as the aircraft approached and penetrated them. Near aircraft lidar observations were much better correlated with in situ sensor observations than lidar observations at greater distances ahead of the aircraft. The major cause of this difference was thought to be the ≈2° offset of the lidar viewing direction from the flight direction. Contrail spatial distributions were not of the quality obtainable from ground-based lidar observations. This results because contrails tend to become horizontally stratified, vertical distance between angular lidar observations increases with increased distance from the aircraft, and erratic aircraft motions during an angular scan.

The most useful lidar observations were made with lidar viewing directions of vertically upward or vertically downward. These provided real-time information on aircraft altitudes to achieve optimum in situ cloud and contrail sampling. At sampling altitudes, the forward-viewing angular scanning observations were useful for fine-tuning the aircraft altitude for cloud and contrail penetration. Best information on cloud and contrail properties were obtained from vertically directed lidar observations as the aircraft performed a series of upward and downward penetrations of contrails. This operational mode was especially well suited for lidar and radiometric evaluation of cloud and contrail optical and radiative properties. The vertical viewing lidar detected ice crystals thought to be precipitating from an aircraft contrail and their

scavenging by a cirrus cloud layer. The lidar display indicates that the crystals are effective for increasing cirrus cloud density. Vertical angular scanning observations can evaluate the sharp decrease in lidar backscatter for small off-vertical viewing directions that result from horizontally aligned ice crystals and perhaps can provide additional information on crystal shapes.

The ≈2° offset of the lidar viewing direction from the flight direction is thought to have greatly degraded the forward-viewing angular scanning observations and this mode of operation was not fully evaluated. However, the reasoning for this capability remains valid and the angular scan presentations collected during this program justifies modification of the lidar pod for true forward direction lidar viewing during future cloud and contrail studies.

1 INTRODUCTION AND OBJECTIVE

The environmental consequences of subsonic and supersonic aircraft fleets need better definition for input to the design of future aircraft and their operational scenarios. NASA is developing a capability to predict the effects of current and future aircraft on the environment through use of a 3-D model consisting of modular parameterizations of effluent emissions and their microphysical and chemical transformations, dynamic behavior, and radiation budget perturbations. Experimental data are needed to better understand relevant atmospheric processes, to develop quantitative relationships that improve model performance, and to validate model predictions. Model simulations will be used to assess and report the effect of aviation on the environment.

As part of the Atmospheric Effects of Aviation Project (AEAP), NASA formulated an extensive multiaircraft field program termed the subsonic aircraft contrail and cloud effects special study (SUCCESS) to characterize exhaust of aircraft in flight, to investigate aircraft exhaust impacts on cirrus formation processes and radiation budgets, and to develop new instrumentation for use on future field studies. The SUCCESS field program was based from Salina, Kansas, primarily to take advantage of the available atmospheric measurements made at the Atmospheric Radiation Measurements Clouds and Radiation Testbed site located in northern Oklahoma and southern Kansas.

Development of an angular scanning aerosol backscatter lidar installation on the NASA DC-8 research aircraft and its participation in the SUCCESS field experiments was funded by the AEAP program. The proposed lidar would be able to scan angularly from vertically downward to vertically upward, and therefore, be able to detect and measure cloud layers and contrails above, ahead of, and below the DC-8, as illustrated in Figure 1. Lidar range-resolved backscatter signatures would be processed and displayed in pictorial format in real time on the DC-8 video network so that the flight director, flight crew, and other experimenters would have information to position the aircraft and operate onboard in situ sensors to best sample contrails and clouds. The data would be recorded so that the lidar presentations could be used to extend measurements made along the flight path into vertical dimensions.

The proposed objectives of the lidar program are listed below:

- Map contrail and cloud distributions above and below the DC-8 to help establish best in situ sampling altitudes
- Map contrail and cloud vertical distributions ahead of the DC-8 at sampling altitudes
- Provide real-time displays for operational purposes and provide data for establishing sampling paths relative to cloud and contrail distributions
- Analyze contrail and cloud radiative properties with combined lidar and radiometric measurements
- Evaluate aerosol mean particle sizes from two-wavelength (1.06 and 0.53 μm) lidar observations

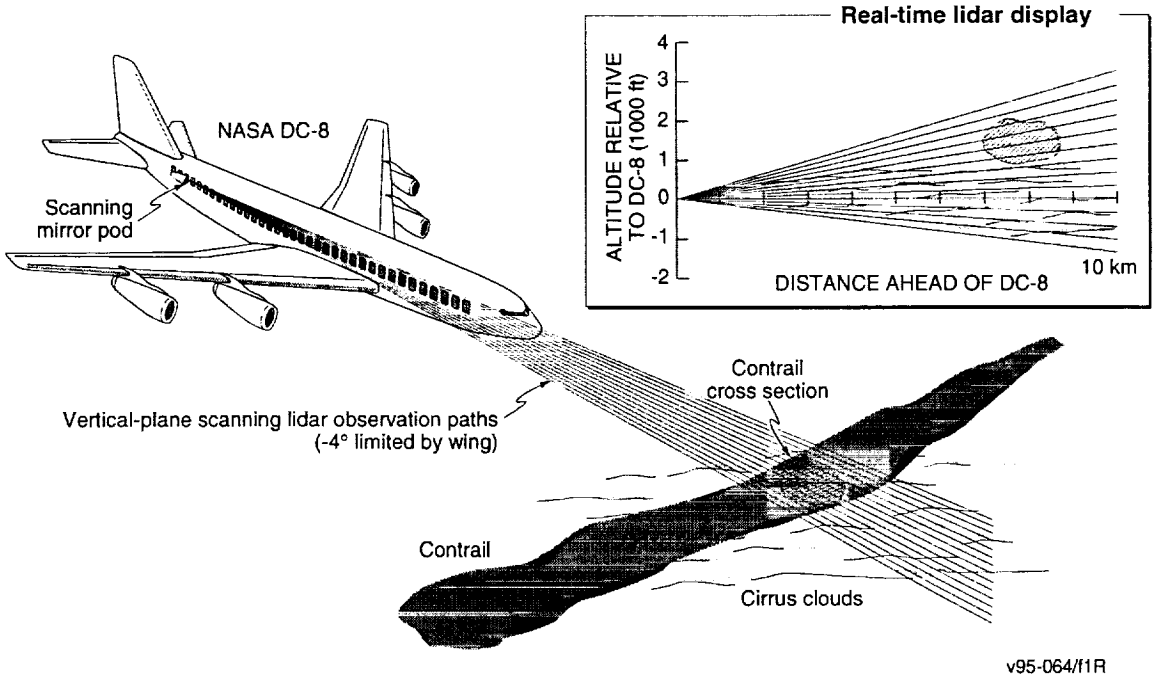

Figure 1. DC-8 scanning lidar operation.

- Study contrail and cloud interactions, diffusion, and mass decay and growth
- Provide a scanning mirror capability for other remote sensing instrumentation.

These objectives were generally achieved, as described by the journal publication presented as Appendix A.

The objective of the current study is to further develop data analysis and display methods appropriate to the DC-8 scanning lidar SUCCESS database and to conduct case study analyses that provide information on contrail and cloud properties.

2 DC-8 SCANNING LIDAR DATABASE

An angular-scanning, large-aperture (36 cm) backscatter lidar was developed and deployed on the NASA DC-8 research aircraft as part of SUCCESS. The lidar viewing direction can be continuously scanned during aircraft flight from vertically upward to forward to vertically downward or at fixed angles. Real-time pictorial displays generated from the lidar signatures were broadcast on the DC-8 video network and used to locate clouds and contrails above, ahead of, and below the DC-8 to depict their spatial structure to help select DC-8 altitudes for achieving optimum sampling by onboard in situ sensors. Several lidar receiver systems and real-time data displays were evaluated to help establish possible lidar configurations and applications on future missions.

The lidar telescope has a 35 cm aperture with a Cassegrain configuration. Backscattered light from atmospheric aerosols is collected by the telescope and divided into two channels by a dichroic beam splitter. After passing through narrowband interference filters to reduce background light levels, the light from each channel is focused onto a solid-state detector. On Channel 1 the 1064 nm detector (3 mm diameter) is enhanced for this wavelength and used in combination with a 60 dB logarithmic amplifier to obtain a large operating dynamic range. Data collected on this channel are primarily for short-range observation while flying directly through cirrus clouds and aircraft contrails. Channel 2 can be used for either the 1064 nm or 532 nm wavelength depending on receiver optical elements. The percentage of energy in each channel can be controlled by the beam splitter. The detector on Channel 2 is smaller in size (0.8 mm) and has more gain and radiant responsitivity. This high-sensitivity channel uses a 40 dB logarithmic amplifier and is used for long-range observation of subvisible clouds. In addition to the data from the two logarithmic channels, linear data from each channel can be digitized and recorded. For special experiments, a polarizer can be added to the 1064 nm channel to differentiate between the crystal structure of cirrus clouds and aircraft contrails.

The lidar data acquisition system is based on an IBM PC. Up to four channels of data can be processed (using Gage Applied Sciences digitizers) and recorded on Exabyte tape. The two linear channels use 12-bit MHz digitizers and the two logarithmic amplifier channels use 8-bit 50 MHz digitizers. A low-speed 8-channel 12-bit A-D card is available for processing signals from associated meteorological sensors such as a narrow-beam radiometer. The DC-8 aircraft flight parameters and related environmental data available on a NASA-supplied data network are input to the lidar data system for recording and presentation on the lidar displays.

A program control unit controls the stepping motor drive of the scanning mirror, and synchronizes it with the laser firing and data acquisition. The motor position is read by the lidar computer and is added to the recorded data array. The lidar data are processed and displayed as color-modulated pictorial displays in real time, on a flat panel VGA color monitor. The video signal passes through a scan converter and is input to the DC-8 video network so that contrail and cloud distributions are available to the mission manager, flight crew, and other experimenters for operational use. The video is also recorded on a HI-8 VCR (>400 line resolution) so that it may be analyzed on standard television receivers.

Following the SUCCESS field program, the lidar data records were transcribed to compact dics (CDs) in a common format to facilitate data transfer to SUCCESS participants and for data analyses. This reduces complications of data use because of hardware and software changes made during the field program. Table 4 lists the lidar database that resides on 37 CDs. The file name contains the date of data collection. Operational times are derived from the DC-8 data network (DADS) and, therefore, missing times listed in Table 1 indicate that the lidar system was not connected to the network.

A condensed log of lidar operational times, angular scan mode, and contrail and cloud observation remarks is given in Table 2. Table 3 presents additional information on lidar configurations and data tape inventory for each SUCCESS flight day. Table 4 lists the digitization range resolution and maximum observational range for each of four lidar backscatter signature channels.

Data selected from the real-time display video recordings were processed for publication quality displays incorporating several standard lidar data corrections. Data examples are presented that illustrate (1) correlation with particulate, gas, and radiometric measurements made by onboard sensors, (2) discrimination and identification among contrails observed by onboard sensors, (3) high-altitude (13 km) scattering layer that exhibits greatly enhanced vertical backscatter relative to off-vertical backscatter, and (4) mapping of vertical distributions of individual precipitating ice crystals and their capture by cloud layers. An angular scan plotting program was developed that accounts for DC-8 pitch and velocity.

The DC-8 scanning lidar methodology and data examples were used to prepare a publication (Appendix A) for the SUCCESS special *Geophysical Research Letters* issue and to generate a web site (www.rsed.sri.com/lidar) linked to the SUCCESS home page that presents results of the study.

Table 1
DC-8 SCANNING LIDAR COMPACT DISC DATABASE

DISC NO.	FILE NAME	START TIME	END TIME
1	96041001.dat	23:55:06	00:52:36
	96041002.dat	23:21:37	23:22:37
	96041301.dat	18:03:29	18:33:52
	96041302.dat	19:11:30	19:36:41
2	96041501.dat	17:53:52	18:48:44
	96041601.dat	17:42:29	19:08:13
	96041602.dat	19:17:04	20:03:27
	96041603.dat	20:08:40	21:04:49
3	96041801.dat	17:30:43	19:40:01
	96041802.dat	19:47:58	20:24:01
4	96042001.dat	: :	16:47:33
5	96042002.dat	16:47:33	17:02:53
	96042003.dat	17:29:25	17:32:46
	96042004.dat	17:36:45	18:23:22
	96042005.dat	18:52:24	19:22:08
	96042006.dat	19:45:15	20:46:39
6	96042007.dat	18:28:06	18:47:53
	96042101.dat	17:53:49	18:31:58
	96042102.dat	18:48:38	18:49:06
	96042103.dat	18:53:04	19:01:11
	96042104.dat	: :	: :
	96042105.dat	: :	: :
	96042106.dat	: :	: :
	96042107.dat	: :	: :
7	96042108.dat	0:51:08	21:03:21
	96042109.dat	20:51:08	21:03:21
	96042110.dat	21:09:00	22:32:54
	96042401.dat	17:06:14	17:33:59
	96042402.dat	17:38:24	18:50:27
	96042403.dat	18:54:22	19:30:44
	96042404.dat	19:38:46	19:45:27
	96042405.dat	19:50:24	20:55:58
	96042406.dat	21:02:23	22:06:35

Table 1
DC-8 SCANNING LIDAR COMPACT DISC DATABASE (continued)

DISC NO.	FILE NAME	START TIME	END TIME
8	96042407.dat	22:12:18	22:30:13
	96042408.dat	22:34:35	23:24:34
	96042701.dat	16:43:59	18:34:05
9	96042702.dat	18:34:06	20:56:59
10	96042703.dat	20:56:59	22:14:02
	96042901.dat	19:23:30	19:44:36
	96043002.dat	18:09:01	18:25:36
11	96043001.dat	17:24:48	18:03:55
12	96043003.dat	18:25:36	19:02:59
13	96043004.dat	19:07:44	23:14:20
	96050201.dat	16:37:25	16:54:00
14	96050202.dat	16:54:00	18:16:14
	96050301.dat	19:31:41	20:29:35
15	96050302.dat	20:29:35	22:08:55
16	96050303.dat	22:08:55	22:29:09
	96050401.dat	17:33:12	17:44:55
17	96050402.dat	17:44:55	19:48:48
18	96050403.dat	19:48:48	20:58:37
19	96050404.dat	20:58:37	21:33:50
20	96050405.dat	21:33:50	21:35:48
	96050801.dat	17:19:02	17:53:02
21	96050802.dat	17:53:02	18:29:36
22	96050803.dat	18:29:36	19:06:59
23	6050804.dat	19:06:59	19:49:22
24	96050805.dat	19:49:22	20:24:02

Table 1
DC-8 SCANNING LIDAR COMPACT DISC DATABASE (concluded)

DISC NO.	FILE NAME	START TIME	END TIME
25	96050806.dat	20:24:02	20:53:17
	96050701.dat	18:18:37	18:20:39
26	96051001.dat	14:37:40	15:19:52
27	96051002.dat	15:19:52	16:12:58
28	96051003.dat	16:12:58	16:43:58
	96051501.dat	19:48:11	20:08:29
29	96051201.dat	20:18:02	23:14:37
30	96051202.dat	23:14:37	23:48:29
31	96051203.dat	23:48:29	0:21:39
32	96051204.dat	0:21:39	0:45:31
33	96051502.dat	20:08:29	20:47:17
34	96051503.dat	20:47:17	22:31:05
35	96051504.dat	22:31:06	23:23:09
36	96051505.dat	23:23:09	23:57:12
37	96051506.dat	3:26:28	0:00:28

Table 2
DC-8 SCANNING LIDAR SUCCESS OPERATIONS LOG

TIME (GMT) START	END	SCAN* ANGLE (°)	REMARKS
4/10/96			
2355	0053	–3, +5	IR on Ch1, green on Ch2;mapping of DC-8 contrail
4/13/96			
1803	1835	+90	Clouds and contrails above aircraft
1911	1929	–3, 5	Couds above aircraft
4/15/96			
1754	1849	–90	Boundary layer clouds only; 1.5 km AGL
4/16/96			
1742	1800	–3. 0	Aircraft approaching clouds
1800	1805	–3, 10	Clouds
1805	1906	–3, 0	Clouds
1917	1936	–3, 10	Aircraft approaching clouds
1936	1950	–3, 10	Mostly clear
1958	2002	–3, 10	Mostly clear; contrail
2008	2015	–3, 10	Mostly clear
2030	2048	–3, 5	IR on Ch1 and Ch2; mostly clouds above aircraft
2057	2105	–3, 2	Clouds penetrated by aircraft
4/18/96			
1731	1750	–3, 0	Clear
1750	1802	–3, 5	Clear
1808	1843	+90	Clear/T-39 ahead DC-8
1925	1932	–3, 5	Clear
1932	2024	–4, 5	Mostly clear; some clouds penetrated
4/20/96			
1547	1601	–4, 4	Mostly clear
1601	1625	0, 10	Cloud layer above aircraft
1625	1703	0, 8	Clouds above; cloud penetrations near 1700 Z
1750	1732	0, 10	Thin layer above
1736	1758	0, 10	Cloud penetrations
1758	1858	–4, 10	Cloud penetrations; 5 Hz rate at 1852
1858	1920	0, 10	Cloud penetrations; 5 Hz rate
1920	1922	0, 8	Cloud penetrations; 5 Hz rate
1945	2024	0, 10	Back at 10 Hz; cloud penetrations
2025	2047	0	Map of clouds; contrails ahead of aircraft

*90° vertically upward, 0° forward, and -90° vertically downward viewing.

Table 2
DC-8 SCANNING LIDAR SUCCESS OPERATIONS LOG (continued)

TIME (GMT) START	END	SCAN ANGLE (°)	REMARKS
4/21/96			
1753	1815	–1, 9	Cloud layer above aircraft
1815	1822	–4, 10	Cloud penetrations
1822	1824	–1, 10	Cloud layer above aircraft
1824	1834	–4, 10	Cloud penetrations; denser above aircraft
1853	1902	–4, 10	Cloud layer above; penetrate cumulus tops
1912	*	–4, 8	DADS disconnected; DC–8 contrails
2051	2125	–4, 8	DADS on; cloud and contrails penetration
4/24/96			
1706	1712	–4, 1	Cloud penetrations by aircraft
1712	1725	–4, 7	Cloud and contrail penetrations
1725	1726	–4, 4	
1732	1753	0, 10	Aircraft approaching and penetrating clouds
1828	1903	0, 5	Cloud and contrail penetrations
1903	1945	–1, 5	Cloud penetrations; some contrails?
2031	2055	+90	Cloud layer above aircraft; in cloud ~2052
2102	2115	0, 8	Cloud penetrations
2122	2133	–2, 6	Cloud penetrations by aircraft
2145	2157	0, 5	Cloud penetrations by aircraft
2201	2220	–90	Cloud layer extends to 2 km below aircraft
2225	2254	–3, 5	Cloud and contrail penetrations
2302	2324	0	Forward viewing cloud penetrations
4/27/96			
1644	1831	–4, 5	T-39 contrail penetrations
1831	1834	–4, 10	
1834	1855	–2, 10	Cloud penetrations
1856	1857	–4, 10	Cloud layer above aircraft
1857	1918	–4, 5	Mostly clear
1918	1937	–4, 10	Cloud penetrations; contrails?
1937	2016	–4, 5	Cloud top penetrations; DC-8 contrail
2027	2122	–4, 5	Mostly clear; some clouds
2122	2144	–4, 10	Cloud layer mostly above aircraft
2144	2145	–4, 8	Low density cloud penetrations
2145	2149	–4, 10	Low density cloud penetrations

Table 2
DC-8 SCANNING LIDAR SUCCESS OPERATIONS LOG (continued)

TIME (GMT) START	TIME (GMT) END	SCAN ANGLE (°)	REMARKS
4/27/96 (cont.)			
2150	2156	+90	Thin cloud near aircraft
2156	2157	–4, 21	Wide sector scan; some clouds at aircraft altitude
2157	2214	–4, 10	Cloud penetrations
4/29/96			
1923	1938	+90	Clear above aircraft
1939	1944	–4, 3	Clear ahead of aircraft
4/30/96			
1728	1747	–4, 4	Clear; contrail
1748	1804	–2, 0	Clear
1809	2314	+90	Clear with occasional widespread thin layers <3 km above aircraft; some layer penetrations
5/2/96			
1637	1740	+90	1637 layer 6 km above; 1706 layer 0.5 km above; 1717–1735 aircraft in layer
1805	1816	+90	Many stratified layers and contrails; convective Cloud tops 3 km above surface
5/3/96			
1932	1946	–4, 4	Clear with 757 contrail returns
2023	2034	–4, 4	Clear with 757 contrail returns
2141	2229	–90	Mostly clear; haze layer near surface; layer 1–2 km Below aircraft after 2204; layer penetration 2227
5/4/96			
1733	1737	+90	IR only Ch1; clear
1737	1749	+90	Green on; layer 3–4 km above; 757 contrail cross sections
1858	2046	–4, 0	IR Ch1 and Ch 2/many 757 contrails; no clouds
2054	2136	–90	Mostly low clouds (2 km above surface); cloud layer 3 km below aircraft 2126–2131 and 2135
5/7/96			
1818	1821	+90	Contrail 1 km above; lidar shut down by flight operations over Denver space

Table 2
DC-8 SCANNING LIDAR SUCCESS OPERATIONS LOG (continued)

TIME (GMT) START	END	SCAN ANGLE (°)	REMARKS
5/8/97			
1719	1749	+90	IR Ch1 and Ch 2; layer 4–5 km above at start; penetration of layer near 1727; clear above after 1735
1749	1823	–90	Clear except clouds near surface
1823	1841	+90	Cloud layer extending to about 1 km above aircraft
1845	1931	+90	Clear
1931	2005	+90	Cloud layer just below aircraft; cloud layer penetration near 1940; clear after 1942
2005	2045	+90	Cloud layer extending to about 1 km above; clear after 2041
2046	2053	–90	Cloud layer near surface; layer 1 km below at 2050; possible penetration of layer 2052
5/10/96			
1436	1644	+90	IR Ch1 and 2/data gaps during aircraft turns; widespread 43,000 ft layer; layer return greatly decreases with non-zenith viewing indicating ice crystals
5/12/96			
2018	2055	+90	IR on Ch1 and Ch 2; mostly clear above aircraft; some thin layers (contrails?)
2250	2302	+90	Layer extending from aircraft upward to about 0.5 km
2313	2445	–90	Complex distributions of cloud, contrails, and precipitating ice crystals extending to about 3 km below aircraft; multiple DC-8 contrails from oval flight pattern; aircraft penetrations of cloud and contrails
5/15/97			
1948	2022	+90	IR on Ch 1 and Ch2; thin layer just below aircraft/appears aircraft penetrates layer
2023	2116	–90	Multiple layers; mostly dense layer (2 km thick) at varying distances (3 to 8 km) below aircraft (6 to 8 km above surface)
2205	2248	+90	Mostly clear above aircraft; some cloud patches near (at) aircraft altitude
2248	2255	+90	Layer from aircraft to 1 km below

Table 2
DC-8 SCANNING LIDAR SUCCESS OPERATIONS LOG (concluded)

TIME (GMT) START	TIME (GMT) END	SCAN ANGLE (°)	REMARKS
5/15/97			
2255	2301	+90	Clear above aircraft
2301	2321	+90	Layer within 1 km below aircraft
2321	2323	+90	Clear above aircraft
2331	2400	–90	Multiple very thin layers; dense layer begins 2342 2 km below aircraft; cloud penetration 2358 to about 2400 GMT

Table 3
DC-8 SCANNING LIDAR SUCCESS CONFIGURATION AND DATA INVENTORY SUMMARY

DATE 1996	DAY	FLIGHT	TAPE INVENTORY NASA VIDEO[1]	TAPE INVENTORY SRI VIDEO[2]	TAPE INVENTORY SRI DATA[3]	RECEIVER BEAMSPLITTER 60 dB/40 dB	RECEIVER WAVELENGTH 60 dB/40 dB	DATA COLLECTION PROGRAM	REMARKS
4/10	101	960201	0	1	2	10%/90%	IR/G	GO1	G and IR radar plots: fixed angle vertical in km, horizontal in time/scan vertical in 1000 ft, horizontal in time.
4/13	104	960202	1	1	3	10%/90%	IR/G	GO1	
4/15	106	960203	1	1	1	10%/90%	IR/G	GO1	
4/16	107	960204	1	2	3	10%/90%	IR/G, IR/IR	GO1	IR/IR > 2030 GMT.
4/18	109	960205	1	1	2	10%/90%	IR/G	GO1	
4/20	111	960206	1	3	6	Dichroic	IR/G	G01	5 Hz lidar rate tested (1352–1426 Z).
4/21	112	960207	2	1	10	Dichroic	IR/G	GO3/GO2	GO3 and GO2 did not fix computer problem GO3 introduced missed shots problem/DADS not recorded on some data.
4/24	115	960208	2	3	8	Dichroic	IR/G	GO3	
4/27	118	960209	2	3	1	Dichroic	IR/G	GO16	New IR receiver installed/computer failure problem fixed. New plots 5000 ft interval A-scope, 5000 ft interval fixed angle.
4/29	120	960210	2	3	1	Dichroic	IR/G	GO17	Varied dB/V on plots.
4/30	121	960211	2	2	3	Dichroic	IR/G	GO17	Adjusted G (40 dB) detector gains. Changed recording ranges requiring tape changes.
5/2	123	960212	2	1	1	Dichroic	IR/G	GO17	
5/3	124	960213	1	2	1	Dichroic	IR/G, IR/IR	GO17	
5/4	125	960214	1	2	1	10%/90%	IR/IR, IR/G	GO17	IR/IR to 1737 Z, IR/G to 1858 Z, IR/IR.
5/7	128	960215	1	0	1	10%/90%	IR/IR	GO17	Only few minutes of operation allowed.
5/8	129	960216	1	2	1	10%/90%	IR/IR	GO17	Receiver calibration.
5/10	131	960217	1	1	1	10%/90%	IR/IR	GO17	Changed grayscale setting to better view high-altitude layer (above DC-8 ceiling).
5/12	133	960218	1	2	1	10%/90%	IR/IR	GO17	
5/15	136	960219	1	2	1	10%/90%	IR/IR	GO17	Adjusted 40 dB detector gains depending on signal strength.

[1]VCR/VHS [2]VCR/HI-8 mm [3]8 mm Exabyte

Table 4

DC-8 SCANNING LIDAR DATA DIGITIZATION SUMMARY

SUCCESS PROJECT (NASA) DATA COLLECTION SUMMARY

			Number of Points/Shot				Sample Interval (ns)				Range (km)			
Date	File Base Name	Tape Number	IR-LOG	GREEN-LOG	IR-LINEAR	GREEN-LINEAR	IR-LOG	GREEN-LOG	IR-LINEAR	GREEN-LINEAR	IR-LOG	GREEN-LOG	IR-LINEAR	GREEN-LINEAR
10-Apr-96	96101	1	5000	5000	808	808	20	20	33	33	15	15	4	4
		2	5000	5000	808	808	20	20	33	33	15	15	4	4
13-Apr-96	96104	1	5000	5000	606	606	20	20	33	33	15	15	3	3
		2	5000	5000	606	606	20	20	33	33	15	15	3	3
		3												
15-Apr-96	96106	1	3333	3333	202	202	20	20	33	33	10	10	1	1
16-Apr-96	96107	1	5000	5000	1010	1010	20	20	33	33	15	15	5	5
		2	5000	5000	1010	1010	20	20	33	33	15	15	5	5
		3	5000	5000	1010	1010	20	20	33	33	15	15	5	5
18-Apr-96	96109	1	5000	5000	1010	1010	20	20	33	33	15	15	5	5
		2	5000	5000	1010	1010	20	20	33	33	15	15	5	5
20-Apr-96	96111	1	5000	5000	3030	1010	20	20	33	33	15	15	5	5
		2	5000	5000	2020	202	20	20	33	33	15	15	15	5
		3	5000	5000	2020	202	20	20	33	33	15	15	10	1
		4	5000	5000	1010	202	20	20	33	33	15	15	10	1
		5	5000	5000	1010	202	20	20	33	33	15	15	5	1
		6	4333	4333	404	202	20	20	33	33	15	15	5	1
21-Apr-96	96112	1	5000	5000	1010	202	20	20	33	33	13	13	2	1
		2	5000	5000	1010	202	20	20	33	33	15	15	5	1
		3	5000	5000	1010	202	20	20	33	33	15	15	5	1
		4	5000	5000	1010	202	20	20	33	33	15	15	5	1
		5	5000	5000	1010	202	20	20	33	33	15	15	5	1
		6	5000	5000	1010	202	20	20	33	33	15	15	5	1
		7	5000	5000	1010	202	20	20	33	33	15	15	5	1
		8	6666	6666	1212	1212	20	20	33	33	15	15	5	1
		9	6666	6666	1212	1212	20	20	33	33	20	20	6	6
		10	5000	5000	1010	202	20	20	33	33	20	20	6	6
24-Apr-96	96115	1	5000	5000	4	4	20	20	6700	6700	15	15	5	1
		2	5000	5000	4	4	20	20	6700	6700	15	15	4	4
		3	5000	5000	4	4	20	20	6700	6700	15	15	4	4
		4	5000	5000	4	4	20	20	6700	6700	15	15	4	4
		5	5000	5000	4	4	20	20	6700	6700	15	15	4	4
		6	5000	5000	4	4	20	20	6700	6700	15	15	4	4
		7	5000	5000	4	4	20	20	6700	6700	15	15	4	4

Table 4

DC-8 SCANNING LIDAR DATA DIGITIZATION SUMMARY
(concluded)

SUCCESS PROJECT (NASA) DATA COLLECTION SUMMARY

Date	File Base Name	Tape Number	Number of Points/Shot				Sample Interval (ns)				Range (km)			
			IR-LOG	GREEN-LOG	IR-LINEAR	GREEN-LINEAR	IR-LOG	GREEN-LOG	IR-LINEAR	GREEN-LINEAR	IR-LOG	GREEN-LOG	IR-LINEAR	GREEN-LINEAR
		8	5000	5000	4	4	20	20	6700	6700	15	15	4	4
27-Apr-96	96118	1	5000	5000	2352		20	20	17		15	15	8	
29-Apr-96	96120	1	1333	1333	1568		20	20	17		4	4	4	
30-Apr-96	96121	1	11768	11768	492		20	20	17		35	35	1	
		2	6666	6666	492		20	20	17		20	20	1	
		3	3333	3333	1960		20	20	17		10	10	5	
2-May-96	96123	1	3333	3333	4021		20	20	17		10	10	10	
3-May-96	96124	1	5333	5333	6274		20	20	17		16	16	16	
4-May-96	96125	1	5000	5000	5882		20	20	17		15	15	15	
7-May-96	96128	1	5000	5000	5882		20	20	17		15	15	15	
8-May-96	96129	1	5000	5000	5882		20	20	17		15	15	15	
10-May-96	96131	1	5000	5000	5882		20	20	17		15	15	15	
12-May-96	96133	1	5000	5000	5882		20	20	17		15	15	15	
15-May-96	96136	1	5000	5000	5882		20	20	17		15	15	15	
Totals														

3 DATA PROCESSING METHODS

The initial lidar data analyses were directed to data records collected with a fixed viewing angle, typically vertically upward or downward. These analyses established a high correlation between lidar and onboard in situ observations. At times, the aircraft conducted vertical penetrations of cloud layers and contrails (Appendix A). However, vertical penetration flight patterns accounted for only a small percentage of the sampling periods, and the most desired data were collected while the DC-8 trailed directly behind emission aircraft. Real-time lidar displays of forward-viewing angular-scan observations indicated excellent contrail detection at long ranges (>10 km), but indicated poor contrail detection at shorter ranges. The initial post field program data analyses indicated the poor real-time forward-viewing lidar performance was caused by a combination of incorrect range correction, uncorrected effects of aircraft motions, and need for improved polar scan display generation. Because the SUCCESS DC-8 lidar is unique from previous DC-8 lidar systems in its scan capability, these angular scan problems need solution for the system to become operational on future field studies. The major objective of the current project was to develop improved scanning lidar data analyses and display techniques and to apply these techniques to evaluate cloud and contrail properties from the SUCCESS database. A secondary objective was to establish the enhanced capabilities of an airborne scanning lidar for use on future atmospheric research programs.

The computer system used for the initial scanning lidar data analyses, as presented in Appendix A, was enhanced by increasing the computational speed and memory size required for efficient processing of large lidar data arrays. New MATLAB instructions were used to generate polar plots in reasonable processing times. Improvements were made to identify and quantify time gaps in the lidar database and to normalize lidar signatures relative to clear-air lidar signatures. A unique method of integrating the lidar angular scan displays with onboard in situ sensor data records was developed. Basically, the aircraft velocity was used to propagate the onboard sensor measurements to distances ahead of the DC-8 so that they could be plotted on the lidar range-dependent displays. Individual angular scan displays were then integrated into a movie format and transferred to web site www.rsed.sri.com/lidar so that they could be played with typical VCR frame processing controls. The reader is encouraged to view these web site displays as they are not presented in this report.

4 CASE STUDY ANALYSES

The movie format described above in Section 3 has been applied to over 36 case studies, which are available at the SUCCESS DC-8 scanning lidar web site (www.rsed.sri.com/lidar). In addition, each case study presents a plot of aircraft altitude and location and a time and range plot of lidar signatures (e.g., without viewing direction consideration). The 36 case studies are listed in Table 5. The case studies are discussed below based on the web site displays.

10 April 1996, 00:45 to 00:53 GMT

The first test flight of the SUCCESS DC-8 instrumentation was conducted on 10 April 1996. During a time of repetitive DC-8 turns, the angular scanning lidar detected two series of DC-8 contrails ahead of the aircraft as the aircraft approached the contrails. The lidar was recording data to 15 km range while making forward-viewing angular scans. The lidar detected the contrail at a range of about 15 km and on successive scans during the 00:44:59 to 00:46:28 GMT time interval as the aircraft closed distance with the contrail. The onboard sensors did not indicate aircraft penetration of the contrail. The second series of contrail observations occurred during the 00:49:21 to 00:50:48 GMT period. The lidar again detected the contrail at distances of about 15 km and at shorter distances as the aircraft closed on the contrail (seven scans). An onboard, in situ, ice water content sensor detected the contrail, and, using the aircraft velocity to propagate the detection ahead of the aircraft, shows good range correlation between the lidar and in situ sensor (00:49:58 to 00:50:11 GMT lidar scan). The NO_y data were not recorded; however, the aircraft log notes that the contrail was observed by the NO_y sensor at 00:51:03 GMT in good agreement with the time of contrail penetration by the DC-8 as inferred from the lidar scans.

These first data proved the concept of the lidar finding contrails at extended distances as an aid to help direct the DC-8 into contrails for their in situ chemical and particle characterization.

16 April 1996, 17:48 to 17:50 GMT

The lidar detected several particulate scattering features at a distance of 14 km ahead of the DC-8. Small angular scans were conducted (–0.6° to 2.5°) so that many angular scans were collected. Distance to the scattering feature decreased with each scan until the aircraft penetrated the scattering feature. The onboard water content sensor shows a large increase at the time of aircraft penetration; however, the NO_y sensor showed no increase indicating that the scattering feature was a cloud not associated with aircraft emissions. During aircraft penetration of dense cloud volumes, the lidar backscatter is highly attenuated so that distant scattering volumes are not observed. As the aircraft leaves the cloud, the lidar again observed at remote distances and shows no cloud volumes. However, the in situ water content sensor requires significant time to recover to clear air readings. The above described features are better observed on the lidar range and time display than on the movie display indicating decreased correlation between lidar and in situ data records as the in situ measurements are propagated ahead of the aircraft using the aircraft velocity. This can be expected as it is more probable that common volumes are observed by the two sensors at closer distances to the observed volumes.

Table 5
ANGULAR SCANNING DC-8 LIDAR CASE STUDIES

Case Study	Date (1996)	Time (GMT)
1	4/10	00:44:59–00:52:29
2	4/13	19:11:37–19:28:32
3	4/16	17:46:31–17:50:12
4	4/16	18:05:11–18:33:08
5	4/16	18:40:29–18:54:58
6	4/16	18:59:29–19:08:10
7	4/16	19:17:11–19:35:54
8	4/16	19:38:04–19:42:04
9	4/16	19:58:42–20:02:32
10	4/16	20:08:51–20:10:23
11	4/16	20:33:35–20:46:51
12	4/18	19:48:12–19:55:32
13	4/18	19:55:45–20:10:51
14	4/20	16:03:01–16:16:58
15	4/20	16:50:04–17:02:33
16	4/20	17:37:00–17:56:54
17	4/20	17:57:09–18:23:08
18	4/20	18:52:36–19:21:55
19	4/21	17:53:56–18:10:49
20	4/21	18:10:50–18:31:50
21	4/21	18:53:21–19:00:51
22	4/21	19:54:52–19:56:49
23	4/21	20:51:15–21:03:03
24	4/21	21:09:06–21:16:52
25	4/24	17:08:37–17:23:54
26	4/24	17:38:40–17:49:06
27	4/24	19:12:07–19:26:52
28	4/24	21:02:33–21:12:54
29	4/24	22:44:10–23:01:01
30	4/27	17:19:09–17:32:53
31	4/27	19:33:07–19:54:51
32	4/27	21:05:08–21:09:29
33	5/03	20:24:59–20:29:34
34	5/04	18:59:02–19:05:53
35	5/04	19:54:47–20:04:52
36	5/04	20:07:21–20:09:21

16 April 1996, 18:05 to 20:47 GMT

The other 16 April 1996 case studies (4 through 11) are similar to the 17:48:30 to 17:50:12 GMT study discussed above. The range and time lidar cross sections show very good correlation with the onboard in situ ice water content sensor CVI. The lidar detects particulate clouds at remote distances when no nearby clouds attenuate the laser energy and tracks the clouds to shorter distances ahead of the aircraft as the aircraft approaches the clouds. At the time the lidar indicates that the aircraft penetrates the cloud, the water content sensor normally also indicates the cloud penetration. Only a few NO_y measurement spikes indicate the presence of aircraft contrails. Near 19:19 GMT, a NO_y spike occurs at the same time as a large ice water content reading that is much wider than the NO_y spike. The lidar returns are attenuated, indicating a dense cloud, and show no correlation with the NO_y readings. An NO_y spike is observed at about 19:14:30 GMT with no indication of a scattering event by the lidar or the onboard ice water sensor. The lidar maps a thin cloud layer about 1 km above and ahead of the aircraft near the end of the 20:33:35 to 20:46:51 GMT case study. Also, comparison of the lidar and CVI sensor records show the slow recovery of the CVI sensor following a high ice water content reading.

18 April 1996, 19:48 to 20:11 GMT

On 18 April 1996, the DC-8 trailed behind the NASA T-39 aircraft to measure its emissions. However, during this time period, the DC-8 scanning lidar was required to observe vertically upward, and no contrail observations were made. Later, forward angular scanning observations made during the time period 19:48:12 to 20:10:51 GMT detected small patchy clouds. Typically, the lidar detected the clouds at a range of about 14 km (the maximum range settings during this time) and mapped the vertical distribution of the clouds as they approached the aircraft. At the time of cloud penetration by the aircraft, as indicated by the lidar, the ice water content sensors (CVI and PVM) typically responded. The movie format with the water content values propagated ahead of the aircraft using recorded DC-8 velocities agree well with the position of the clouds measured by the lidar. These data indicate that the lidar is more sensitive to detection of small clouds than are the onboard ice water content sensors. This is well illustrated by the movie format for the 18 April 1996 case studies available on the www.rsed.sri.com/lidar web site.

20 April 1996, 16:03 to 19:22 GMT

During the 16:03 to 16:17 GMT period (case study 14), no scattering targets were detected at or near the aircraft altitude. The onboard ice water content sensors verified no clouds were penetrated by the DC-8. The lidar detected thin (≈9.5 km) clouds 1 to 2 km above the aircraft. During 16:50 to 17:02 GMT, clouds were observed above the aircraft with some penetrations by the aircraft verified by the ice water content sensors. These lower density clouds did not significantly attenuate the lidar signal. No contrails were penetrated by the aircraft according to the NO_y record. During 18:53 to 19:01 GMT, the cloud frequency greatly increased from the earlier sampling times and the cloud densities increased and the range of lidar observations decreased. The aircraft did not penetrate any contrails according to the NO_y record. The 17:57 to 18:23 GMT lidar scans are characterized by scattering volumes penetrated by the aircraft. However, the scattering volumes are only occasionally observed by the onboard ice water content sensors. Near 18:30 GMT, a strong NO_y spike is recorded indicting aircraft penetration

of an aircraft contrail. This is not observed by the ice water content sensors but appears to have been detected by the lidar. After 18:16 GMT, the lidar signal is attenuated by high density clouds ahead of the aircraft. The aircraft penetrated a few clouds during the 18:52 to 19:22 GMT (case study 18), but the lidar movie format shows that most of the clouds were just above the aircraft.

21 April 1996, 17:54 to 18:11 GMT

Case study 19 (17:54 to 18:11 GMT) is characterized by lidar detected clouds above the DC-8 and no cloud or contrail penetrations by the aircraft. Clouds above the aircraft were also observed during the 18:11 to 18:32 GMT (study 20) and 18:53 to 19:10 GMT (study 21) periods, but some cloud penetrations by the DC-8 occurred with good agreement between times of penetration by the lidar and in situ sensors.

Many contrails generated by the DC-8 were observed by the forward scanning lidar and onboard NO_y and ice water content sensors during the 19:55 to 19:57 GMT period. Lidar detection ranges of 10 km are achieved, but mostly shorter detection ranges ($\approx$1 km) are obtained, probably because of the circular flight patterns of the DC-8 to intersect its own contrail (see the flight pattern plot for case study 22). We do not know the visibility of these contrails, so the question of lidar detection of subvisible contrails needs further investigation. Although the lidar mapped contrail spatial distributions, these are not as dramatic as the contrail cross sections obtained by NASA using a ground-based lidar. This results because the contrails quickly become horizontally stratified and, therefore, the forward-viewing lidar must observe the thin part of the contrail. Also, the vertical distance between angular measurements increases with range from the aircraft. Small erratic aircraft motions during an angular scan also degrades the spatial mapping of small contrails.

At 21:10 GMT, a thin horizontal contrail was observed by the lidar ahead of the aircraft and the aircraft appeared to penetrate the contrail; this was verified by the onboard NO_y sensor. The contrail was not detected by the in situ water content sensor.

24 April 1996, 17:98 to 23:01 GMT

The DC-8 penetrated a combination of clouds and contrails during the 17:08 to 17:24 GMT period as interpreted by the lidar and in situ NO_y and ice water content sensors. The lidar angular scan made from 17:18:49 to 17:19:04 shows a very patchy contrail, and this is verified by the NO_y onboard in situ sensor with a data record showing three concentration peaks as the DC-8 traverses the contrail. The 17:38 to 17:49 GMT case study is dominated by a dense cloud that attenuates the lidar signal. Several contrails were penetrated by the DC-8 during the 19:12 to 19:27 GMT interval. The contrails are difficult to distinguish from clouds by the lidar and in situ water content sensors—it appears that several contrails are embedded within clouds. Clouds were penetrated by the aircraft during the 24 April 1996 21:02 to 23:01 GMT case study with no indication of contrails. According to the NO_y sensor, about nine contrails were penetrated by the DC-8 during the 22:44 to 23:01 GMT sampling period. Many more scattering features are detected by the lidar and ice water content sensors indicating contrails embedded within clouds, although scattering features could be contrails not detected by the NO_y sensor.

27 April 1996; 17:19 to 21:09 GMT

On 27 April 1996, the DC-8 trailed behind the NASA T-39 aircraft to sample its contrails. Many contrail penetrations occurred during the 17:19 to 17:33 GMT period of case study 30. The lidar observed the contrails to a distance of 2 km. It is believed that longer range contrail observations were not achieved because of the small size of the contrails along the contrail axis and because the lidar beam was offset a few degrees from the forward direction in order to miss any samplers extending from the DC-8 fuselage—the lidar was installed in the rear of the DC-8 so as to allow space for the many DC-8 in situ sensors employed on the SUCCESS mission. These results clearly show the capability of the lidar to detect and map contrails at remote distances. We believe these contrails were subvisible, but this is uncertain. Because of the small size of the contrails, different sampling locations of the in situ sensors on the DC-8, and the angular offset of the lidar, as well as turbulent movement of the DC-8 when trailing another aircraft, the time correlation between contrail observations is degraded. Nevertheless, individual contrail samples can be distinguished on the data records. These data indicate a higher sensitivity of the lidar to contrail detection than the ice water content sensors, probably because of higher sampling time resolution for observing small-sized contrails. The lidar angular cross sections provide information on contrail vertical distributions as illustrated by several frames of the movie format for case study 30.

During the 19:33 to 19:55 GMT period (case study 31), the DC-8 flew a series of spiral flight patterns in order to sample its own contrail. The lidar was able to detect these contrails to a distance of about 10 km, possibly limited by the flight path geometry. The ice water content sensors did not seem to respond to these contrails.

At about 21:07 GMT (case study 32), the lidar detected a scattering feature extending from a distance of 8 to 14 km ahead of the DC-8. On five consecutive angular scans, the scattering feature was approached by the aircraft. At the time of aircraft penetration estimated from the lidar scans, the NO_y sensor record shows a narrow peak reading indicating that a contrail was being sampled. The ice water content sensor shows a broader response but not as wide as indicated by the lidar. The lidar angular scan movie format (web site) indicates that the DC-8 was just below the contrail, which may explain the narrow peaks of the NO_y and ice water content sensors. By combining these data records, a better value of total contrail gas and particulate concentrations should be achieved.

A larger NO_y peak at 21:06:30 GMT was not observed by the lidar or water content sensors.

3 May 1996, 20:25 to 20:30 GMT

The DC-8 trailed behind the NASA 757 aircraft on 3 May 1996 in order to sample its near aircraft emissions. Case study 33 (20:25 to 20:30 GMT) shows a high correlation between the NO_y and CVI onboard sensor records and indicates the DC-8 was in the 757 contrail most of the time. The lidar shows only a few contrail returns, mostly at ranges less than 1 km ahead of the DC-8. This may result because of the close distance of the DC-8 to the 757 and the few degrees offset from the forward direction of the lidar viewing angle.

4 May 1996, 18:59 to 20:09 GMT

On 4 May 1996, the DC-8 again trailed the 757 to sample its emissions. The distance between the two aircraft was increased (to about 10 miles) from that of 3 May 1996 so that a

larger aircraft emission plume could be expected. During case study 34 (18:58:59 to 19:05:57 GMT), the NO_y sensor shows many narrow peak returns as does the PVM ice water content sensor. The CVI ice water content sensor indicates the DC-8 was almost continuously within the 757 emissions plume. The lidar returns are mostly at ranges less than 1 km with occasional returns to 3 km and indicates the DC-8 was almost continuously within the 757 emissions plume. We again believe this indicates the lidar can observe the emissions at remote distances with high sensitivity, but that the few degrees offset of the lidar viewing direction from the aircraft flight direction greatly reduces the probability of the laser beam intersecting the contrail of an aircraft directly ahead of the DC-8 at extended distances.

Case study 35 (19:54:41 to 20:04:59 GMT) is similar to case study 34 discussed above and clearly demonstrates the lidar capability to detect the 757 emissions at remote distances with some returns to 4 km—but probably limited by viewing geometry as discussed above.

Case study 36 presents lidar angular scans of several contrails detected at extended distances ($\approx$10 km) from the DC-8 and at shorter distances as the aircraft approached the contrails. The movie format shows that the contrails passed just above the DC-8 and were not detected by the onboard in situ sensors.

5 CONCLUSIONS AND RECOMMENDATIONS

SUCCESS afforded the opportunity to develop and apply an angular scanning lidar from the NASA DC-8 atmospheric research aircraft. The lidar was able to map particulate backscatter above, ahead of, and below the DC-8 in real time for operational purposes to best position the aircraft for in situ atmospheric sampling. The recorded lidar records are also useful for interpretation of data collected from in situ and radiometric sensors and for inferring optical and radiative properties of clouds and contrails. Several interesting data products derived from fixed viewing angle lidar observations relating to the AEAP have been presented in a journal publication (Appendix A). However, other vertical viewing lidar systems are available for installation on the DC-8 and the value of the angular scan lidar must be judged by the usefulness of the forward-viewing angular scan observations. For inferring contrail and cloud properties, the following are concluded from the SUCCESS scanning lidar program.

- Real-time displays of contrail and cloud locations and distributions were provided to help direct aircraft flight and in situ measurement operations. Vertical upward and downward viewing observations were more useful for establishing flight altitudes than forward-viewing angular scan observations. However, once the flight altitude was selected, the angular scan observations were more useful for fine-tuning aircraft altitude for penetration of scattering volumes.
- The lidar proved effective for detection of aircraft contrails to remote distances of at least 15 km in clear sky conditions. Detection ranges greatly decreased in cloudy conditions as the lidar energy was attenuated by the clouds.
- Forward-viewing lidar detected clouds and contrails at short detection ranges are relatively well correlated with cloud and contrail detection by onboard in situ sensors. The correlation greatly decreases for longer lidar detection ranges, probably a result of the $\approx 2^\circ$ offset from forward viewing of the lidar and small erratic motions of the aircraft resulting in different atmospheric volumes being sampled. The higher sampling resolution of the lidar over the ice water sensors and near-cloud attenuation of greater distance lidar observations also decrease correlations between lidar and in situ observations.
- Airborne forward-viewing observations of contrails do not provide as good of information on contrail spatial distributions as does ground-based lidar. This results because contrails tend to become horizontally stratified, the vertical distance between angular measurements increases with distance from the aircraft, and there are erratic aircraft motions during an angular scan.
- Analyses of the fixed viewing direction (Appendix A) and angular scanning (web site) lidar observations, indicate that when combined with in situ sensor measurements, vertical lidar observations provide more information on cloud and contrail properties than forward-viewing angular scanning observations. The best sampling scenario is with a vertical viewing lidar and aircraft upward and downward penetrations of the cloud and contrail (see Figures 4 and 5 of Appendix A).

- Vertical and near vertical lidar observations of high-altitude cirrus clouds show a sharp decrease in lidar backscatter at small angles from the vertical (Figure 6 of Appendix A). This is explained by horizontally aligned ice crystals. Therefore, apparent variations in cloud density from a vertical pointing lidar may not be related to actual cloud density variations, and the use of a viewing angle offset from the vertical will provide better mapping of cloud density structure. Also, a scanning lidar such as the SUCCESS DC-8 system may provide important information on crystal size and shape properties.
- The most interesting DC-8 lidar data showed intense scattering from individual precipitating ice crystals, probably from a contrail, and their scavenging by a cirrus cloud layer (Figure 7 of Appendix A). This observation was possible because of horizontally shaped ice crystals (with enhanced backscatter) and the relatively short lidar range (i.e., high energy density of the diverging laser beam). The data indicate that cloud density is increased by the precipitating crystals.

Study results and conclusions may not seem to justify the increased complexity of the scanning lidar over vertical or near vertical pointing lidar installation on the DC-8. However, we believe benefits of the scanning lidar approach were not fully explored because of the angular offset of the laser beam from the forward direction. The final configuration of in situ sensor installations for SUCCESS would have allowed true forward viewing (or within a few tenths of a degree offset). Unfortunately, this may require substantial modification of the scanning mirror pod. Several recent proposals submitted to NASA for development of the scanning lidar were unsuccessful because it was viewed that the airborne scanning lidar is not a new sensor development. We believe reasoning for the DC-8 scanning lidar is still valid but recommend that the pod modification be made before any future applications.

6 PUBLICATIONS AND PRESENTATIONS

6.1 JOURNAL PUBLICATIONS

Aviation Week and Space Technology, 1996: "NASA completes tests on airborne lidar," AW&ST, 29 July 1996.

E.E Uthe, N.B. Nielsen, and T.E. Osberg, 1998: "Airborne scanning lidar observations of aircraft contrails and cirrus clouds during SUCCESS," GRL, Vol. 25, pp. 1339–1342, (See Appendix A.)

6.2 CONFERENCE PRESENTATIONS

N.B. Nielsen, E.E. Uthe, R.D. Kaiser, M.A. Tucker, J.E. Baloun, and J.G. Gorords, 1996: "NASA DC-8 airborne scanning lidar sensor development," Proceedings Second International Airborne Remote Sensing Conference and Exhibition, San Francisco, California, 24–27 June 1996. Available from ERIM International, Ann Arbor, Michigan 48113-4008.

N.B. Nielsen and E.E. Uthe, 1996: "NASA DC-8 airborne scanning lidar system," 18th International Laser Radar Conference, 22–26 July 1996, Berlin, Germany.

E.E. Uthe, T.E. Osberg, and N.B. Nielsen, 1997: "NASA DC-8 airborne scanning lidar cloud and contrail observations," Proceedings, Cloud Impacts on DoD Operations and Systems 1997 Conference (CIDOS-7), 23–25 September 1997, Newport, RI. Phillips Laboratory, Directorate of Geophysics, Hansom AFB, Massachusetts 01731-3010.

E.E. Uthe, 1997: "NASA DC-8 airborne scanning lidar operation during SASS/SUCCESS," Abstract Volume, 1997 Conference on the Atmospheric Effects of Aviation, 10–14 March 1977, Virginia Beach, Virginia.

E.E Uthe, 1998: Airborne scanning lidar applications to global atmospheric chemistry field studies. Abstracts Volume, CAGGP/IGAC Symposium on Global Atmospheric Chemistry, 19–25 August 1998, Seattle, Washington.

Uthe, E.E., 1998: "Airborne sensors data fusion: Aerosol/cloud properties," Aerosol Forcing Science Team Meeting, Goddard Space Institute, New York, New York, 18–20 November 1998. Abstract at web site (http://www.giss.nasa.gov/gacp/science_team/).

APPENDIX A

AIRBORNE SCANNING LIDAR OBSERVATIONS OF AIRCRAFT CONTRAILS AND CIRRUS CLOUDS DURING SUCCESS (GRL, VOL. 25, PP. 1339–1342, MAY 1 1998)

GEOPHYSICAL RESEARCH LETTERS, VOL. 25, NO. 9, PAGES 1339-1342, MAY 1, 1998

Airborne scanning lidar observations of aircraft contrails and cirrus clouds during SUCCESS

Edward E. Uthe, Norman B. Nielsen, Terje E. Osberg

SRI International, Menlo Park, California

Abstract. An angular scanning backscatter lidar was deployed on the NASA DC-8 research aircraft as part of SUCCESS. The lidar viewing direction could be continuously scanned from vertically upward to forward to vertically downward. Real-time pictorial displays generated from lidar signatures were used to locate clouds and contrails above, ahead of, and below the DC-8; to depict their spatial structure; and to help select DC-8 altitudes for achieving optimum sampling by onboard in situ sensors. The lidar data are being analyzed to establish their value in the interpretation and extension of the in situ sensor databases. Data examples are presented that illustrate (1) correlation with particulate, gas, and radiometric measurements made by onboard sensors, (2) discrimination and identification between contrails observed by the onboard sensors, (3) a 13.1 km altitude layer that exhibits greatly enhanced vertical backscatter relative to off-vertical backscatter, and (4) mapping of vertical distributions of individual precipitating ice crystals and their capture by cloud layers.

Introduction

The Atmospheric Effects of Aviation Project (AEAP) has formulated and conducted field studies to better understand the environmental consequences of effluent emissions from subsonic and supersonic aircraft. The Subsonic Aircraft: Contrail and Cloud Effects Special Study (SUCCESS) employed four NASA aircraft based from Salina, Kansas, during April and May 1996. The DC-8 research aircraft provided a platform from which a large number of state-of-the-art aerosol, chemical, and radiometric sensors could be operated in a manner that allowed for sampling of effluent emissions from aircraft during flight in the upper troposphere. However, a method was needed to help locate and direct the DC-8 into thin cirrus cloud layers and compact aircraft contrails, and to provide high spatial resolution data on the vertical structure of clouds and contrails sampled along the aircraft flight path. For this purpose, a DC-8 scanning lidar design was approved for development by the AEAP for use on SUCCESS in the manner illustrated by Figure 1.

Lidar Design

Relatively minor modifications were made to an existing lidar sensor for its installation on the DC-8. The lidar employs a laser transmitter producing 275 mJ energy pulses at a wavelength of 1.064 μm, or about 130 mJ at each of the 1.064 and 0.532 μm wavelengths transmitted simultaneously with a pulse rate of 10 Hz. A 35-cm diameter Cassegrain telescope collects backscattered light and a beam splitter divides the received light into two channels that can be configured for multiwavelength, polarization, or extended dynamic range detection. Resulting signals are logarithmically amplified and digitized by 8-bit 50-MHz (3 m range resolution) transient recorders. Digital records are stored on Exabyte 8-mm tape and are computer processed for real-time pictorial display in several formats. The displays were scan converted to NTSC video and input to the DC-8 video network for viewing by both the flight crew and experimenters for flight direction and data collection operational purposes.

The major effort in the DC-8 installation was the development of the scanning capability. The lidar was installed within the aircraft and viewed outward from an open side window. A pressurized scanner pod consisting of a 45-degree mirror and a 43-cm diameter window was mounted within a motor-driven and computer-controlled rotating cylinder that was attached to the DC-8 fuselage. A fixed position aerodynamic fairing was also attached to the fuselage and located to the rear of the scanner pod to allow the lidar viewing direction to be scanned from vertically upward to forward in the direction of aircraft travel to vertically downward. Figure 2 pictures the scanning lidar pod/fairing installed near the DC-8 tail section (the forward sections of the aircraft are best used by the in situ sensors). Other details of the lidar and lidar installation have been discussed by *Nielsen et al.* [1996].

Lidar Operation and Real-Time Displays

Typically, the scanning lidar was operated in a downward or upward vertical viewing direction to determine the presence, altitude, and thickness of particulate layers above and below the aircraft to help establish in situ sampling altitudes. At sampling altitudes, the lidar normally performed forward viewing angular scan patterns to map the vertical structure of clouds and contrails ahead of the aircraft. Two examples of the real-time angular scan video display are shown in Figure 3. The upper display of each example presents an intensity-modulated picture of cloud structure generated from the 1.06 μm wavelength lidar data with the vertical axis in 1000 ft intervals and the horizontal axis in 1 km intervals—a range of 15 km in these displays. (Note: To facilitate operational use, the altitude scale was displayed in units of kft rather than km at the request of the aircraft pilots. Therefore, the data displays presented in this paper deviate from the scientific metric convention.) The lower display of each example presents lidar logarithmic signal intensity at 0.53 and 1.06 μm wavelengths as a function of range from the lidar (lidar signature) for the last signature plotted in the upper part of the display. The lower text box gives information on scan number, time, aircraft altitude, pitch of the aircraft, and the lidar viewing angle for the last lidar signature plotted. The laser produced 10 signatures per second and the scan mirror was rotated at 1° per second. Typically, a scan was generated every 10 to 15 seconds depending on the angular sector being scanned. A second, real-time intensity-modulated display with range and time axes was used for fixed angle viewing.

Paper number 97GL03612.
0094-8534/98/97GL-03612$05.00

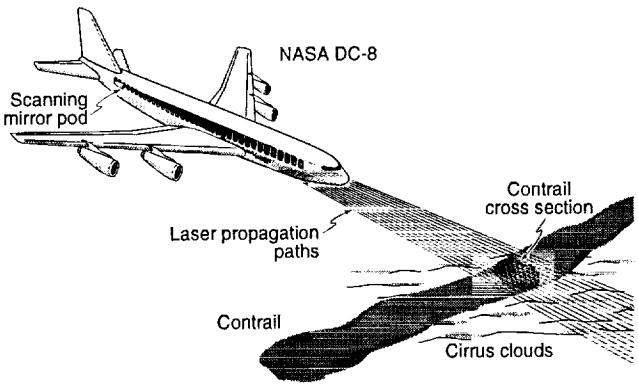

Figure 1. DC-8 scanning lidar illustration.

The primary purpose of the scanning lidar was to provide real-time data on cloud/contrail spatial distributions for flight direction operations. However, all digital data records were recorded on 8-mm magnetic tape for use in subsequent data analyses programs.

Data Analysis Examples

Forward looking angular scan displays provided information on the vertical distribution of clouds and contrails ahead of the DC-8. However, several problems confront this mode of operation and data display. The display is distorted because of aircraft travel during the angular scan. For a 10° sector, the aircraft normally travels about 2 km between the first and last lidar observation of the scan. Moreover, when the DC-8 trailed behind another aircraft as a means to sample its emissions, wake vortices generated by the test aircraft introduced erratic DC-8 motions that translated into lidar pointing jitters so that cloud and contrail targets could not be uniformly scanned. A computer program is being developed to at least partially correct for aircraft travel and erratic motions. The data examples presented below were developed from fixed viewing angle observations.

During 12 May 1996, the DC-8 sampled its own contrail by flying a series of oval-shaped orbits. During the second orbit the DC-8 repeatedly penetrated the contrail generated during the first orbit by increasing and decreasing its altitude in a sinusoidal pattern. Figure 4 presents DC-8 lidar data collected with a fixed downward viewing direction and shows the contrail just below the DC-8 at times the DC-8 was above the contrail with other aerosol layers below. Above the lidar data display are plotted corresponding time histories of liquid water content, NO_y gas concentration, radiometric infrared blackbody temperature (narrow-beam downward-pointing radiometer), and upwelling solar flux (relative units) as measured by onboard sensors and supplied by other experimenters (see Acknowledgments). The lidar display clearly depicts times when the contrail is below the aircraft and indicates times when the aircraft penetrated the contrail. These times agree well with times of observed increased water content and NO_y concentrations. The combined lidar and in situ observations establish times the contrail was above the aircraft as indicated in Figure 4. The radiometric data agree with this analysis showing cooler IR temperature and increased upwelling solar flux at times when the contrail was below the aircraft. Although the solar radiometric data have not yet been calibrated or corrected for aircraft motions, it appears that the albedo is increased by about 30% by the presence of the contrail.

Figure 2. DC-8 scanning lidar pod and aerodynamic fairing installation with pod positioned for forward lidar viewing.

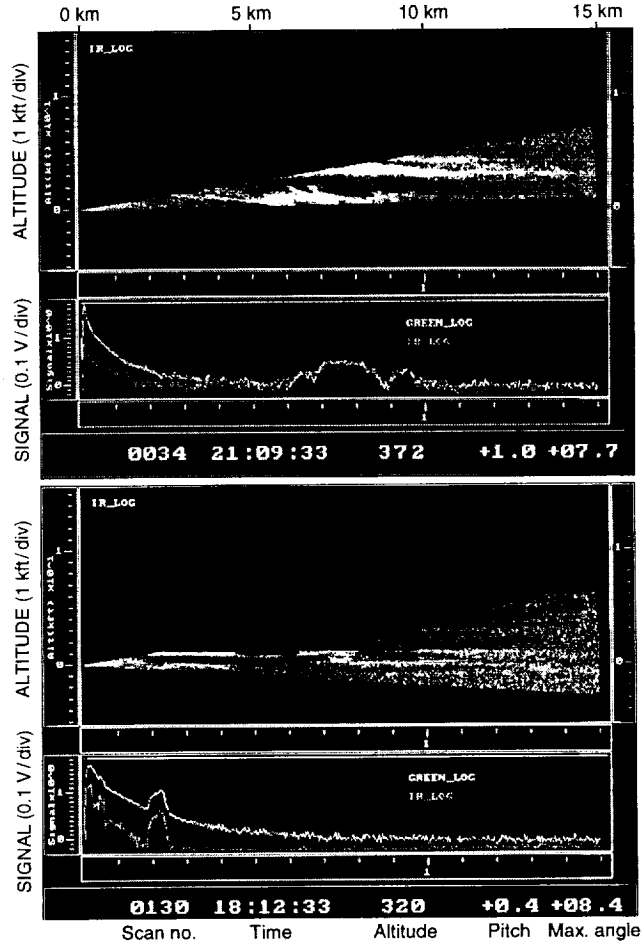

Figure 3. Real-time angular scan video displays generated by the DC-8 scanning lidar system.

Figure 5 presents data collected several minutes after that of Figure 4. The NO_y data again indicate that the scattering feature observed directly below the DC-8 resulted from aircraft emissions. Times when the lidar indicates contrail penetration by the DC-8 again agree with the time history of data collected from the onboard in situ and radiometric sensors. However, at 23:26:30 GMT the lidar observed two distinct contrails at different altitudes, with the first contrail sampled by the onboard sensors at 23:27:00 GMT and the second contrail sampled by the sensors at times after 23:27:10 GMT. It appears that the NO_y to water

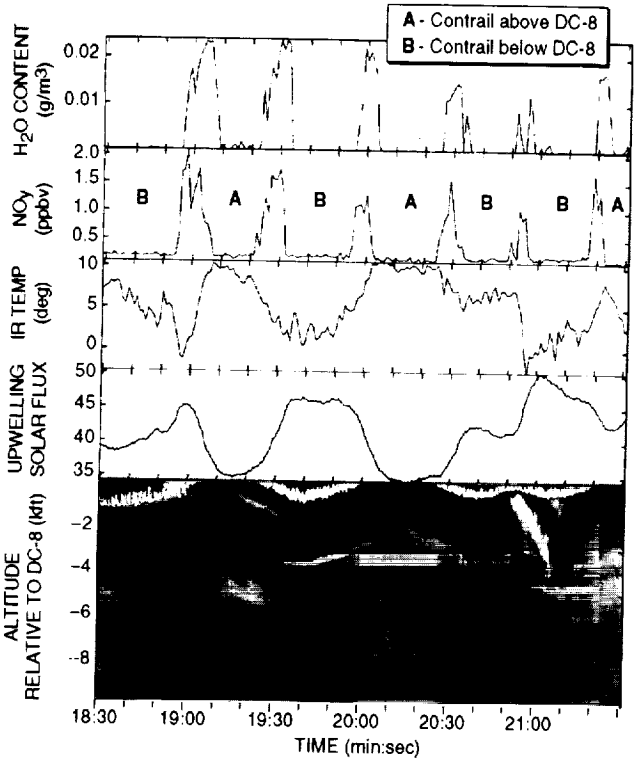

Figure 4. Lidar and selected in situ and radiometric data at times of the DC-8 penetrating its earlier generated contrail, 12 May 1996, 23:18:30 to 23:21:30 GMT. DC-8 altitude approximately 11 km (36 kft).

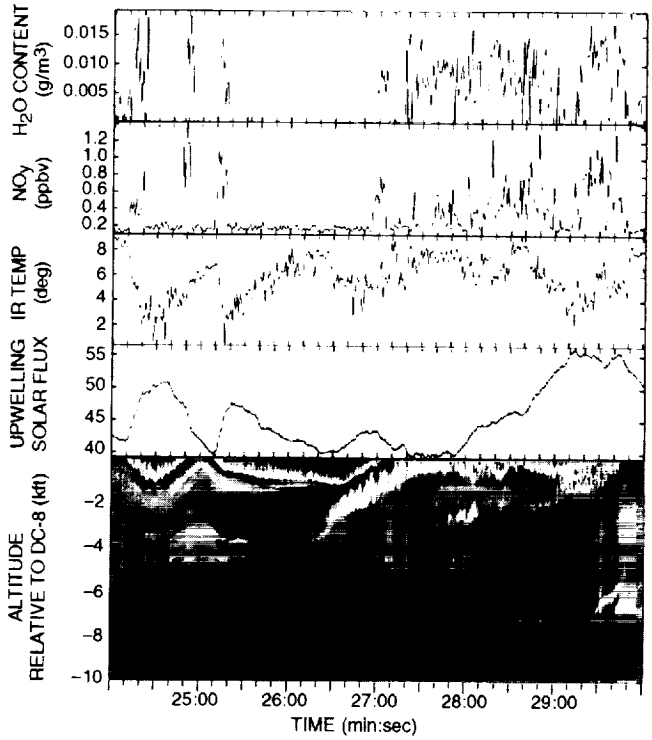

Figure 5. Lidar and selected in situ and radiometric data at times of the DC-8 penetrating its earlier generated contrail, 12 May 1996, 23:24:00 to 23:30:00 GMT. DC-8 altitude approximately 11 km (36 kft).

content ratio is smaller for the later sampled contrail. An analysis of the DC-8 flight paths indicates that the first sampled contrail resulted from the first DC-8 orbit and the later sampled contrail resulted from the second DC-8 orbit. Without the lidar data, this distinction between different aged contrails being sampled by the in situ sensors may have gone unnoticed.

On 10 May 1996, the lidar observed over a large regional area a thin scattering layer at an altitude of about 13.1 km (43,000 ft) MSL—above the flight ceiling of the DC-8 during this flight. Figure 6 presents upward viewing lidar returns from the layer before and after an aircraft turn that was made at an aircraft altitude of about 5.2 km (17,000 ft) MSL. The backscatter from the particulate layer sharply decreases as the aircraft turn is initiated and the laser pulses intersected the layer at nonvertical angles. This behavior has been observed by one of the authors for high-altitude tropical cirrus [*Uthe and Russell,* 1977] consisting of horizontally aligned plate-shaped ice crystals, and has been observed by several other lidar researchers [*Intrieri et al.,* 1995; *Thomas et al.,* 1990]. The rate of backscatter decrease with angle is dependent on size, shape, and orientation of the crystals [*Platt,* 1978]. The scanning lidar provides a means to measure the zenith-enhanced backscatter without aircraft turns that affect other measurements such as solar and infrared flux. The horizontal alignment has been explained by falling crystals orienting themselves to offer maximum resistance to motion [*Platt,* 1978].

It may be possible to detect individual precipitating crystals with lidar—especially if horizontally aligned precipitating crystals are viewed by a vertically pointing lidar at relatively short ranges from the lidar before significant beam divergence occurs. Figure 7 presents vertically downward viewing lidar data collected on 12 May during a time period in which precipitating ice crystals were noted by other experimenters. The lidar plot shows many one-pixel strong returns (speckles) above the cloud located near 1.2 km (4,000 ft) below the DC-8 altitude of 11.9 km (39,000 ft) and no strong returns superimposed on the clear-air returns below the cloud indicating the crystals are completely scavenged by the cloud. Clear air returns below the cloud indicate that the absence

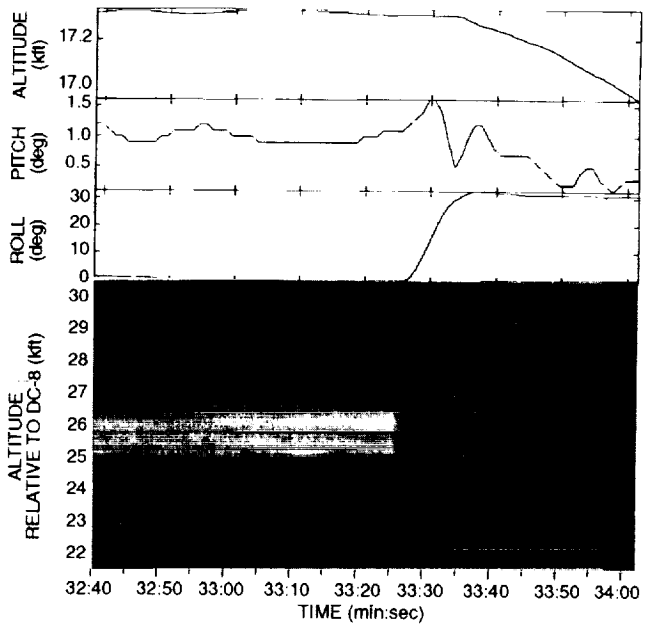

Figure 6. DC-8 lidar observations and selected DC-8 flight parameters showing a sharp decrease in lidar backscatter from a high altitude (43 kft/13.1 km) layer at small angles from the vertical, 10 May 1996, 16:32:40 to 16:34:05 GMT.

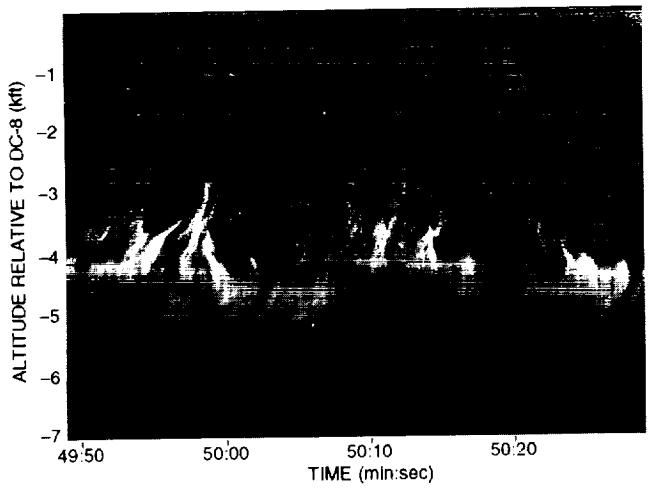

Figure 7. DC-8 downward viewing lidar observations showing intense single-pixel returns from precipitating ice crystals that are scavenged by a cirrus cloud layer, 12 May 1996, 23:49:50 to 23:50:29 GMT. DC-8 altitude approximately 39 kft (11.9 km).

of the speckles is not caused by cloud attenuation of the laser energy. The DC-8 contrail from an earlier orbit was located above the DC-8 and was probably the source of the precipitating crystals. The top of the cloud below the aircraft exhibits vertical striations possibly as a result of the influx of precipitating crystals.

The DC-8 scanning lidar can view in the direction of aircraft travel to remotely observe atmospheric volumes the aircraft is about to penetrate and be sampled by onboard in situ aerosol and gas sensors. Most of the forward viewing observations were conducted by scanning the lidar viewing over an angular sector as illustrated by Figure 1 as a means to generate data displays as shown by Figure 3; those observations provide information on the vertical structure of contrails and clouds sampled by the onboard sensors. However, Figure 8 presents a data example with the lidar viewing angle fixed forward in the aircraft flight direction. Onboard in situ sensor data collected at the time the remotely detected aerosol features are penetrated by the DC-8 verifies the scattering features as clouds or contrails. The airborne horizontal lidar viewing facilitates evaluation of atmospheric homogeneity and optical properties [*Measures,* 1984].

Additional data examples are presented at web site address http://www.rsed.sri.com/lidar.

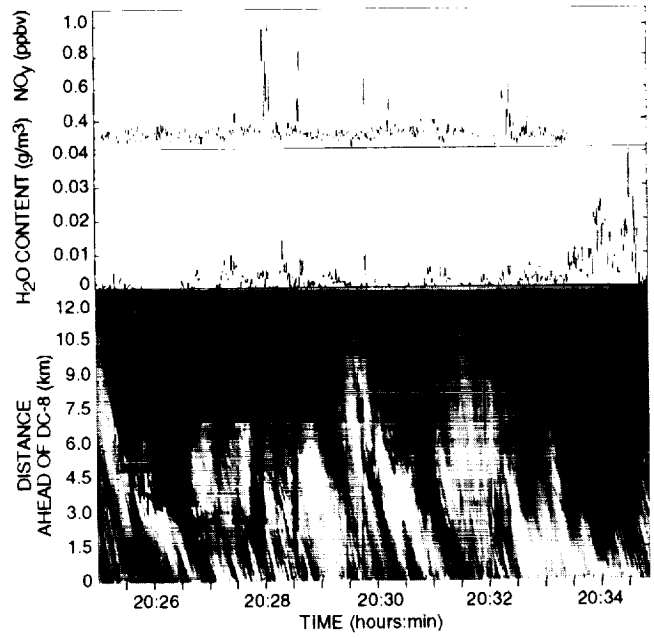

Figure 8. DC-8 fixed-angle forward viewing lidar and selected in situ data, 20 April 1996, 20:25 to 2:35 GMT. DC-8 altitude approximately 37 kft (11.3 km).

Conclusions

SUCCESS afforded the opportunity to develop and apply a scanning lidar from the NASA DC-8 atmospheric research aircraft. The lidar was able to map particulate backscatter above, ahead of, and below the DC-8 in real time for operational purposes to best position the aircraft for in situ atmospheric sampling. The recorded lidar records are also useful for interpretation of data collected from in situ and radiometric sensors and for inferring optical and radiative properties of clouds and contrails.

Acknowledgments. The SUCCESS DC-8 scanning lidar program was funded under Cooperative Agreement NCC2-885 with the NASA Ames Research Center. The water content data were provided by *H. Gerber* [personal communication, 1997; *Gerber et al.,* 1998], the NO_y data by *A. Weinheimer* [personal communication, 1997; *Ridley et al.,* 1994], and the solar flux records by *F. Valero and A. Bucholtz* [personal communication, 1997; *Valero et al.,* 1997]. A. Heymsfield suggested and encouraged analysis of the 12 May data, which proved beneficial to the program. The authors thank the many NASA DC-8 research facility staff and contractors who helped design, develop, and install the scanning lidar system, and the SUCCESS management team for their patience and support during system development.

References

Gerber, H. et al., Measurement of wave cloud microphysics with two new aircraft probes, *Geophys. Res. Lett.*, this issue, 1998.

Intrieri, J.M. et al., Multiwavelength observations of a developing cloud system: The FIRE II 26 November 1991 core study, *J. Atmos. Sci.*, 4079–4093, 1995.

Measures, R.M., *Laser Remote Sensing Fundamentals and Applications,* John Wiley and Sons, New York, 1984.

Nielsen, N.B. et al., NASA DC-8 airborne scanning lidar sensor development, Proceedings of the Second International Airborne Remote Sensing Conference and Exhibition, San Francisco, CA, 24–27 June 1996.

Platt, C.M.R., Lidar backscatter from horizontal ice crystal plates, *J. Appl. Meteor.*, 482–488, 1978.

Ridley, B.A. et al., Distributions of NO, NO_x, NO_y, and O_3 to 12 km altitude during the summer monsoon season over New Mexico, *J. Geophys. Res.*, 99, 25519–25534, 1994.

Thomas, L. et al., Lidar observations of the horizontal orientation of ice crystals in cirrus clouds, *Tellus*, 211–216, 1990.

Uthe, E.E. and P.B. Russell, Lidar observations of tropical high-altitude cirrus clouds, *Radiation in the Atmosphere,* H.J. Bolle (Editor), Science Press, Princeton, New Jersey, 242–244, 1977.

Valero, F.P.J. et al., The Atmospheric Radiation Measurements Enhanced Shortwave Experiment (ARESE): experimental and data details, submitted to *J. Geophys. Res.*, 1997.

Edward E. Uthe, Norman B. Nielsen, and Terje E. Osberg, SRI International, 333 Ravenswood Avenue, Menlo Park, CA 94025 (e-mail: edward_uthe@qm.sri.com)

(Received June 25, 1997; revised November 24, 1997; accepted December 5, 1997.)